Published in final edited form as:

Cancer Lett. 2021 July 10; 510: 79–92. doi:10.1016/j.canlet.2021.04.004.

Dual blockade of EGFR and CDK4/6 delays Head and Neck Squamous Cell Carcinoma Progression by Inducing Metabolic Rewiring

Sanjib Chaudhary[1], **Ramesh Pothuraju**[1], **Satyanarayana Rachagani**[1], **Jawed A. Siddiqui**[1], **Pranita Atri**[1], **Kavita Mallya**[1], **Mohd W. Nasser**[1,9], **Zafar Sayed**[2], **Elizabeth R. Lyden**[3], **Lynette Smith**[3], **Siddhartha D. Gupta**[4], **Ranju Ralhan**[5], **Imayavaramban Lakshmanan**[1], **Dwight T. Jones**[2], **Apar Kishor Ganti**[*,6,7,9], **Muzafar A. Macha**[*,8], **Surinder K. Batra**[*,1,9,10]

[1]Department of Biochemistry and Molecular Biology, University of Nebraska Medical Center, Omaha, NE 68198, USA

[2]Department of Otolaryngology-Head & Neck Surgery, University of Nebraska Medical Center, Omaha, NE 68198, USA

[3]Department of Biostatistics, University of Nebraska Medical Center, Omaha, NE 68198, USA

[4]Department of Pathology, All India Institute of Medical Sciences, New Delhi, India

[5]Department of Otolaryngology-Head & Neck Surgery, Mount Sinai Hospital, Toronto

[6]Department of Internal Medicine, VA Nebraska Western Iowa Health Care System, University of Nebraska Medical Center, Omaha, NE 68198, USA

[7]Department of Internal Medicine, University of Nebraska Medical Center, Omaha, NE 68198, USA

[8]Watson-Crick Center for Molecular Medicine, Islamic University of Science and Technology, Awantipora, Jammu and Kashmir, 192122, India

[9]Fred and Pamela Buffett Cancer Center, University of Nebraska Medical Center, Omaha, NE 68198, USA.

[*]Corresponding authors. Mailing address: **Apar K. Ganti**, MD, University of Nebraska Medical Center, Omaha, Nebraska, 68198-5870 aganti@unmc.edu, **Muzafar A. Macha**, Ph.D., Watson-Crick Center for Molecular Medicine, Islamic University of Science and Technology, Awantipora, Jammu and Kashmir, India 192122 muzafar.aiiims@gmail.com, **Surinder K. Batra**, Ph.D., University of Nebraska Medical Center, Omaha, Nebraska, 68198-5870, USA, sbatra@unmc.edu.

Authors' contributions

Conception and design: M.A.M., S.C., and S.K. B.; Data acquisition and analysis: S.C., R.P., S.R., J.A.S., P.A., K.M., L.S., E.R.L., S.R., S.D.G., and M.A.M; writing and original draft preparation: M.A.M., S.C., and S.K. B.; critical review and editing: S.C., R.P., S.R., J.A.S., P.A., K.M., M.W.N., Z.S., I.L., D.T.J., A.K.G., M.A.M., and S.K.B.; supervision: M.A.M. and S.K.B; funding acquisition: A.K.G. and S.K.B. All authors have seen the final draft of the manuscript before submission.

Conflict of interests

SKB is one of the co-founders of Sanguine Diagnostics and Therapeutics, Inc. AKG has received consulting fees from AstraZeneca, Jazz Pharmaceuticals, G1 Therapeutics, Blueprint Medicines, Genentech, Flagship Biosciences, Mirati Therapeutics and research support form Takeda. AKG also serve on a DSMC for YMAbs. Other authors disclose no potential conflicts of interest.

[10]Eppley Institute for Research in Cancer and Allied Diseases, University of Nebraska Medical Center, Omaha, NE 68198, USA.

Abstract

Despite preclinical success, monotherapies targeting EGFR or cyclin D1-CDK4/6 in Head and Neck squamous cell carcinoma (HNSCC) have shown a limited clinical outcome. Here, we aimed to determine the combined effect of palbociclib (CDK4/6) and afatinib (panEGFR) inhibitors as an effective strategy to target HNSCC. Using the TCGA-HNSCC co-expression analysis, we found that patients with high EGFR and cyclin D1 expression showed enrichment of gene clusters associated with cell-growth, glycolysis, and epithelial to mesenchymal transition processes. Phosphorylated S6 (p-S6), a downstream effector of EGFR and cyclin D1-CDK4/6 signalling, showed a progressive increase from normal oral tissues to leukoplakia and frank malignancy with poor outcome. While increased p-S6 level was drastically reduced during combination treatment in the HNSCC cell lines and mouse models. Combination treatment reduced the cell growth and induced senescence via increasing reactive oxygen species with concurrent ablation of glycolytic and tricarboxylic acid cycle intermediates. Additionally sub-cutaneous and genetically engineered mouse model (K14-CreER^{tam};LSL-Kras^{G12D};Trp53^{R172H}) studies indicated reduction in the tumor growth and delayed tumor progression, respectively. This study collectively demonstrates that dual targeting may be a critical therapeutic strategy in blocking tumor progression via inducing metabolic alteration and warrants clinical evaluation.

1. Introduction

Overexpression or hyperactivation of epidermal growth factor receptor (EGFR) [1–4], cyclin D1 [5, 6] along with simultaneous low levels of cyclin-dependent kinase inhibitor 2A (CDKN2A or p16Ink4a) [7] are the hallmarks of various cancer types, including a majority of head and neck squamous cell carcinoma (HNSCC). This dysregulation is associated with resistance to chemo-radiation therapy (CRT), promotes disease recurrence, and poor prognosis in the HNSCC patients [8, 9]. Despite recent advances in the different treatment modalities in HNSCC, the five-year survival remains at 40–50% [10], and the median age of diagnosis is 63 years [11], thus emphasizing the need to develop new therapeutic strategies to combat the disease.

Oncogenic signals from EGFR and cyclin D1 are known to promote metabolic rewiring in the cancer cells to support the tumor cell survival and progression [12–14]. EGFR mediated metabolic rewiring requires the activation of the Akt/mTOR1 signaling pathway [1]. While cyclin D1 co-ordinates the cellular metabolism to promote cell cycle progression by activating the cyclin-dependent kinases (CDKs) and inhibiting the retinoblastoma (Rb) protein. Rb inactivation then releases the E2 factor 1 (E2F1) to initiate the transcription of target genes that are essential for G1 to S phase progression. However, p16Ink4a (CDKN2A) can inhibit this process by blocking the activity of cyclin D1 and CDK4/6 complexes to allow p-Rb sequester E2F1, thereby inducing the cell cycle arrest [15]. Although targeting CDK4/6 by abemaciclib in mice has some promise in delaying the growth of recurrent tumors, however these tumors showed the retention of cyclin D1 expression to favor tumor growth in a CDK4/6 dependent manner after HER2 withdrawal [16]. In addition, the

blockade of cyclin D1-CDK4/6 complex by abemaciclib also resulted in the activation of EGFR family kinases via mTORC1 activity [16], suggesting the presence of alternative routes for disease progression.

The US Food and Drug Administration approved the anti-EGFR monoclonal antibody, cetuximab, with a limited efficacy of 10–30% only as monotherapy due to the presence of intrinsic resistance [17]. Also the patients with tumor response also developed a subsequent disease progression due to the existence of cetuximab resistance [17]. In addition to intrinsic resistance against anti-EGFR therapy, several alternative mechanisms have been proposed, for example, increased cyclin D1 expression during the resistance to gefitinib in HNSCC [9]. Our previous study targeting EGFR with small molecular inhibitor, afatinib, radio sensitized the HNSCC cells [18]; however, the xenografts non-responsive to therapy indicated increased expression of cyclin D1, CDK4, CDK6, and p-EGFR (Tyr-1068) expression. This observation indicates an intricate signaling network of EGFR and cyclin D1-CDK4/6 complex in HNSCC, which supersedes the mTOR1-SK6-S6 activity to promote tumor cell survival and disease progression. Thus, dual targeting of EGFR and cyclin D1-CDK4/6 may potentially synergize to impede tumor growth and progression in HNSCC. Palbociclib (PD0332991), a small molecule inhibitor of CDK4/6 is proven to have anti-proliferative effects in various types of cancers [19]. It also confers anti-tumor effect by altering the cellular metabolism and reactive oxygen species (ROS) levels, triggering either apoptosis or cellular senescence and modulating the immune response [19]. Currently, many clinical trials to investigate the combined effect of palbociclib with other inhibitors are underway [19]. While in HNSCC, phase II trials combining palbociclib with cetuximab (NCT02499120) and carboplatin (NCT03194373) are currently ongoing. Overall, this study aims to determine the therapeutic potential of afatinib and palbociclib in-combination in the cell lines and preclinical mouse models of HNSCC.

2. Materials and Methods

2.1. *In silico* analysis

Expression analysis of EGFR, cyclin D1, CDK4, and CDK6 were determined in the TCGA HNSCC dataset (http://ualcan.path.uab.edu/, RRID: SCR_015827). Top 150 highly positive co-expressed genes of EGFR and cyclin D1 were analyzed in the dataset extracted from the cBioPortal (https://www.cbioportal.org, RRID: SCR_014555). Pathway enrichment and survival analysis was performed in the Metascape (https://metascape.org, RRID: SCR_016620) and the Kaplan-Meier plotter (https://kmplot.com/analysis/, RRID: SCR_018753) respectively.

2.2. Chemicals and kits

The chemicals and kits used in the study are mentioned in Supplementary Material. All assays are performed following the manufacturer's instructions.

2.3. Cell lines, culture, and treatments

All HNSCC cell lines, UMSCC1 (RRID: CVCL_7707), UMSCC47 (RRID: CVCL_7759) was purchased from the University of Michigan, USA; Cal27 (RRID: CVCL_1107) and

FaDu (RRID: CVCL_1218) was a kind gift from Dr. Prabhat Goswami (University of Iowa Health Care, USA), and immortalized normal oral epithelial cells MoE1a (RRID: CVCL_JE62) and MoE1b (RRID: CVCL_JE63) were cultured as mentioned previously [18, 20]. Cell lines were authenticated by short tandem repeat DNA profiling at the University of Arizona Genetics Core (RRID: SCR_012429) and the Munroe-Meyer Institute, University of Nebraska Medical Center, USA. Treatments with afatinib and palbociclib at various concentrations for 36–48 h were performed in cell lines for various assays.

2.4. Immunohistochemistry and patient samples

Normal (n=28), leukoplakia (n=70) [hyperplasia (n=29), dysplasia (n=41)] and HNSCC (n=95) patient samples were stained with pS6 (Ser-235/236) by immunohistochemistry (IHC). IHC was performed as described earlier [18]. The tissue staining was represented as composite score [21] and optical density (OD) [22].

2.5. Western blot and antibodies

Total protein lysates and western blotting was performed as described previously [21]. Details of antibodies used in the experiments are provided in Supplementary Material.

2.6. Cell viability and colony formation assay

MTT and colony formation assay after drug treatment was determined as described previously [18, 23].

2.7. Drug combination response

The combination response of the drugs (afatinib and palbociclib) were determined based on the ZIP reference model using an online SynergyFinder tool [24]. The detailed procedure as mentioned in the web was followed (https://synergyfinder.fimm.fi/synergy/synfin_docs/#datanal). Synergy scores less than −10 indicates antagonistic; from −10 to 10 indicates additive; while greater than 10 indicates a synergistic interaction between the two drugs.

2.8. Cell cycle analysis

DNA content was measured by flow cytometry as described previously [18].

2.9. Senescence-associated β-galactosidase assay

The β-galactosidase assay was performed as previously described [25].

2.10. Immunofluorescence

Mitochondrial translocases of outer membrane (Tom20) protein was stained in cell line by immunofluorescence as described previously [18].

2.11. Glucose metabolism and ATP assays

Glucose and ATP levels in control and treated cells (palbociclib- 1 and 2.5 μM, afatinib-250 nM, and combination) were analyzed by glucose uptake assay and ATP detection assay kit (Supplementary Material). After 48 h of drug treatments, the glucose and ATP levels were analyzed according to the manufacturer’s instructions.

2.12. Glycolysis and TCA metabolite analysis

Glycolytic intermediates and TCA metabolites were analyzed as previously described [26]. Briefly, UMSCC1 cells (0.3×10^6) seeded in a six-well plate were treated with palbociclib (2.5 μM), afatinib (250 nM), and in combination. After 48 h of treatment, the cells were rapidly rinsed with LC-MS grade water (37°C) and 1 ml of ice-cold methanol:chloroform (9:1) was added to each well while the plates were on ice. Cells were then scraped, centrifuged at 14000g for 3 min and the supernatants were vacuum dried to evaporate the methanol and lyophilized using a freeze-drying system (Labconco, Kansas City, USA). The samples dissolved in LC-MS grade water were analyzed using the API 4000 Triple Quadrupole Mass Spectrometer. Peak areas were normalized to respective biomass and relative metabolite quantification was calculated.

2.13. Murine studies

All animal experiments were reviewed and approved by the IACUC (University of Nebraska Medical Center). Xenograft study was performed as described previously [18, 27]. About 1.5×10^6 viable cells resuspended in 50 μl of PBS were injected in the right and left flank of athymic nude mice (RRID: IMSR_JAX:002019) and allowed to form tumors. After 10 days of injection, tumor volume was measured by Vernier caliper and animals were randomized into four groups- vehicle control, palbociclib (25 mg/kg/day), afatinib (10 mg/kg/day), and combination. Treatments were given by oral gavage. In a genetically engineered mouse model (GEM) of HNSCC: K14-CreER^{tam};LSL-Kras^{G12D};Trp53^{R172H}; Cre was activated in six to eight-week old mice by injecting three doses of tamoxifen (1 mg/mouse/day) to initiate tumor formation [28]. As this model develops squamous cell carcinoma in the tongue within two weeks after tamoxifen injection, the animals were randomized (five animals per group) after 10 days of Cre activation and treatments were carried out for further three weeks as mentioned above. After the treatment endpoint the mice were euthanized, tumors collected, and analyzed for specific proteins by IHC.

2.14. Statistical analysis

Data collected were analyzed using GraphPad Prism (RRID: SCR_002798) software (version 9). Student's *t*-test or ANOVA followed by Tukey's multiple comparisons test was used to calculate statistical significance between the groups. Fisher's exact test was used to assess the association of cytoplasmic p-S6 expression with tissue type and clinicopathological characteristics. Event-free survival was analyzed using the Kaplan-Meier method, and comparisons were done with the Log-rank (Mantel-Cox) test. *P < 0.05, **P < 0.01, ***P < 0.001, and ****P < 0.0001 was considered statistically significant. SAS (RRID: SCR_008567) software version 9.4 was used for IHC analysis (SAS Institute Inc., Cary, NC).

3. Results

3.1. Hyperactive EGFR and cyclin D1-CDK4/6 signaling promote tumorigenesis via gene-clusters that induces cell growth, glycolysis, and EMT

Majority of HNSCC patients harbor EGFR overexpression and are associated with poor disease survival and recurrence [29]. Although EGFR overexpression is associated with the intrinsic resistance in HNSCC [30], the development of alternative routes to evade tumor cell killing is undeniable. Our previous xenograft studies with afatinib (pan-EGFR inhibitor) is shown to radio sensitize the HNSCC cells [17], however the mice that were non-responsive to the therapy indicated an increased expression of cyclin D1, CDK4, and CDK6 as compared to responsive counterparts suggesting its role in therapy resistance (Supplementary Fig. S1). Therefore, we analyzed the genetic alterations of EGFR, cyclin D1, CDK4, and CDK6 in TCGA HNSCC dataset. We observed a significant over-expression of *cyclin D1*, *EGFR*, *CDK4*, and *CDK6* in HNSCC patients (n=520) compared to normal (n=44) along with gene amplification and was associated with poor survival (Supplementary Fig. S2a–c). Next to identify the existence of alternative pathways that promote the progression of HNSCC, we analyzed the co-expressed genes of EGFR (947 genes) and cyclin D1 (288 genes) extracted from the cBioPortal (Fig. 1a). Pathway analysis showed the enrichment of hallmarks of glycolysis, EMT, hypoxia, and cell growth in the EGFR and cyclin D1 co-expressed genes (Fig. 1b & Supplementary Fig. S3).

In addition, we also observed genetic alternations in *EGFR*, *cyclin D1*, *CDK4*, and *CDK6* in the HNSCC patients (Supplementary Fig. S2b). To determine whether these alterations also lead to the activation of EGFR and cyclin D1-CDK4/6 signaling in HNSCC cell lines, we examined the phosphorylated forms of Rb (Ser-780), S6 (Ser-235/236), and mTOR1 (Ser-2448), the downstream targets of respective pathways. The active forms of EGFR (Tyr-1068), mTOR1 (Ser-2448), S6 (Ser-235/236), Rb (Ser-780) were observed along with high levels of cyclin D1, CDK4, and CDK6 in the HNSCC cell lines (Fig. 1c). Such increased levels of p-EGFR (Tyr-1068), cyclin D1, and CDK4/6 were also observed in the tongue tumors of HNSCC mice model [GEM model: K14-CreER^{tam};LSL-Kras^{G12D};Trp53^{R172H} (KKP)] compared to control tissues (Fig. 1d), suggesting its role in tumor progression.

3.2. Activated S6 in HNSCC patients are associated with poor disease prognosis

Phosphorylated S6 (p-S6) is the downstream effector of mammalian target of the rapamycin (mTOR) which regulates cell growth, protein synthesis, glucose hemostasis [31], and is also associated with tumorigenesis [32, 33]. p-S6 at serine (235/236) is shown to serve as a surrogate marker to predict therapy response against HER2 and mTOR1 inhibitors in certain cancers [34, 35]. As EGFR and cyclin D1-CDK4/6 signaling converge via mTOR1 to activate S6K-S6, therefore p-S6 expression may serve as a potential marker for therapy response for both the signalling. Thus, we assessed the p-S6 expression in HNSCC patients (n=95) by IHC and found a progressive increase in cytoplasmic p-S6 staining from normal to premalignant lesions to invasive tumors (Fig. 1e). Of 28 normal tissues, three (10.7%) samples showed reactivity to p-S6 in the epithelial cells, while there was progressive increase in cytoplasmic staining from normal oral tissues to leukoplakia with no dysplasia

[8/29 (27.6%), p=<0.18, OR (95% CI) = 3.2 (0.7 – 13.5)] to leukoplakia with dysplasia [19/41 (46.3%) p=<0.0018, OR (95% CI) = 7.2 (1.9 – 27.6)], and HNSCC [68/95 (71.6%) p=<0.001, OR (95% CI) = 21.0 (5.8 – 75.3)]. Although there was no association between p-S6 expression and other clinicopathological characteristics of the patients; increased p-S6 expression was associated with shorter median disease-free survival of patients (14 months) in contrast to low expression (32 months, p<0.001) (Fig. 1f).

3.3. Afatinib in combination with Palbociclib decreases cell proliferation and induces cell-cycle arrest in HNSCC

Since EGFR and cyclin D1-CDK4/6 signaling is hyperactive in HNSCC cell lines and the KKP mouse model (Fig. 1c & d), we investigated whether these pathways can be co-targeted by afatinib and palbociclib. We treated the HNSCC cell lines (UMSCC1 and Cal27) and normal immortalized oral cells (MoE1a and MoE1b) with both the drugs to determine the effective concentration for 24–48 h. A dose-dependent decrease in the cell viability (Supplementary Fig. S4a) was observed with an effective concentration (IC50) between 0.25 – 1 μM and 1 – 2.5 μM for afatinib and palbociclib respectively. The combinatorial treatment (palbociclib- 1 & 2.5 μM and afatinib- 250 nM) in HNSCC cells (UMSCC1 and Cal27) drastically reduced the cell viability and clonogenic potential of the cells compared to single agent alone, indicating additive effect (synergy score=7.18) of the drugs (Supplementary Fig. S4a & Fig. 2a). This result was further confirmed by flow cytometry analysis; palbociclib caused a cell cycle arrest at G0/G1 of the HNSCC cells (UMSCC1, Cal 27, and FaDu) (Fig. 2b & Supplementary Fig. S4b), which was further enhanced when combined with afatinib (Fig. 2b). No subG0 population was observed during treatments suggesting no apoptosis induction by either drug. In-addition, there was a concurrent decrease in the migration and invasion of UMSCC1 cells during combination compared to single drug treatments (Supplementary Fig. S4c).

To further investigate the growth inhibitory effect at the molecular levels during combination treatment, we analyzed the expression of p-Rb (Ser-807/811), p-S6 (Ser-235/236), p-EGFR (Tyr-1068), cyclin D1, and cyclin E1 after drug treatments in UMSCC1 and Cal27 cell lines. Palbociclib drastically reduced the p-Rb levels, but gradually increased the p-EGFR and p-S6 levels in a dose-dependent manner (Fig. 2c). Intriguingly, cyclin D1 and cyclin E1 levels were also increased during palbociclib treatment suggesting the stabilization of an inactive cyclin D1-CDK4/6 complex (Fig. 2c) with no change in the phosphorylated 70SK (upstream kinase of p-S6) levels (Fig. 2c). Interestingly, afatinib alone or in combination with palbociclib decreased the expression of p-EGFR, cyclin D1, CDK4, and CDK6 in both the cell lines (Fig. 2d). Although afatinib and palbociclib decreased the p-EGFR levels in the normal oral immortalized epithelial lines, MoE1a and MoE1b, there was no change in other proteins (Fig. 2e). Overall, these data highlights the existence of crosstalk between EFGR and cyclin D1-CDK4/6 signalling in HNSCC.

3.4. Combination treatment induces metabolic alteration in HNSCC

EGFR and cyclin D1-CDK4/6 signalling pathways are known to induce transcriptional reprogramming in cancer cells to coordinate cell growth, metabolism, and mitochondrial function for its survival. As our TCGA co-expression analysis (EGFR and cyclin D1)

indicated gene clusters associated with the hallmarks of glycolysis, epithelial to mesenchymal transition, hypoxia, metabolism, and cell growth in HNSCC (Fig. 1c & Supplementary Fig. S3), we investigated the effect of the drugs in cancer cell metabolism. Also targeting CDK4/6 with palbociclib is established to increase cellular complexity by elevating the organelle biosynthesis and cellular metabolism [36]. Thus, to understand the combined effect of palbociclib and afatinib in cellular complexity, we treated the UMSCC1 and Cal27 with either drug or in combination for 48 h. As observed previously [36], our flow cytometer analysis showed increased cell size (forward scatter) and complexity (side scatter) with palbociclib treatment; however, such cellular characteristics were absent during combination (Supplementary Fig. S5).

Variation in the intracellular ATP levels indicates changes in cell metabolism [37, 38]. To determine the effect of palbociclib and afatinib in cell metabolism, we assessed the ATP levels as a function of glycolysis, TCA cycle, and oxidative phosphorylation (OXPHOS). Palbociclib significantly increased the ATP levels; however, this trend was reversed when afatinib was combined with palbociclib or used alone (Fig. 3a). Similarly, glucose uptake by the cells was also increased with palbociclib, but significantly reversed when combined with afatinib (Fig. 3b). Further, to understand the effect of palbociclib and afatinib in metabolic flux, we measured the glycolysis and TCA cycle intermediates by mass spectrometry. We found that palbociclib treatment increased the glycolytic (glucose 6-phosphate, fructose 1,6-bisphosphate, 1,3-bis phosphoglycerate, 3-phosphoglycerate, pyruvate, and lactate production) and TCA metabolites (citrate, α-keto-glutarate, succinate, fumarate, malate, and oxalo-acetate) in UMSCC1 cells (Fig. 3c & d). This increased metabolism due to palbociclib treatment underscores its therapeutic utility in HNSCC; however, the increased glycolysis and TCA cycle were drastically reduced during treatment with afatinib alone or in combination. Western blot analysis also indicated no change in the OXPHOS levels with either palbociclib or afatinib in both UMSCC1 and Cal27 cells (Fig. 3e). These results show that palbociclib addict the cancer cells to induce high ATP production to enhance the cytostatic effect of other agents that affect glucose influx.

Increased levels of mTOR1, RSK (Ser-389), and S6 phosphorylation during palbociclib treatment [36] is associated with increased glycolysis and OXPHOS. In-addition, oncoprotein, cMyc also regulates metabolic reprogramming in a variety of human cancers. We investigated whether the changes in metabolism was also associated with cMyc and mTOR1/S6 signaling. We observed that palbociclib increased the phosphorylation of mTOR1 (Ser-2448), S6 (Ser-235/236), ERK (Thr-202/Tyr-204), and Akt (Ser-473); however, this activation was reduced when it was combined with afatinib (Fig. 3e). Further, the combination also decreased the expression of cMyc and glucose transporter, GLUT1 in HNSCC cells (Fig. 3e).

3.5. Combination treatment induces ROS production and senescence

Decreased cell proliferation coupled with increased cell size and cell cycle arrest is associated with senescence induction [39, 40]. We, therefore investigated the senescence-associated beta-galactosidase (SA-β-gal) activity after drug treatments in HNSCC cell lines. We observed increased SA-β-gal positive cells during combination compared to treatment

with single drugs or control cells, suggesting the cytostatic effect during combination in HNSCC cell lines (Fig. 4a). Interestingly this effect was sustained even after the cells were relieved from drug pressure (Supplementary Fig. S6a).

Inhibiting glucose uptake induces ROS generation by reducing electron transport chain input and depolarization of mitochondrial membrane potential [41], to cause impaired glycolysis, TCA cycle, and OXPHOS function, resulting in cell death or senescence [42]. Therefore, to investigate the role of ROS in increased senescence during combination treatment, we measured the intracellular and mitochondrial ROS in HNSCC cells. We observed an increase trend in the intracellular and mitochondrial ROS with palbociclib, while afatinib had a mild effect (Fig. 4b & Supplementary Fig. S6b). Interestingly, ROS production was further increased when palbociclib was combined with afatinib (Fig. 4b & Supplementary Fig. S6b). To further illustrate the mechanism of increased ROS production, we measured the mitochondrial mass and membrane potential by Tom20 and JC-1 staining respectively. Although palbociclib had no effect on Tom20, mitochondrial membrane potential was increased compared to control cells. Although combination had no effect on mitochondrial mass, but the number of functional mitochondria was significantly decreased (Fig. 4c & d).

To further delineate the mechanism of increased ROS production during combination treatment despite low functional mitochondria, we analyzed the expression of antioxidant enzymes- MnSOD (SOD1), Cu/ZnSOD (SOD2), extracellular Cu/ZnSOD (SOD3), NAD(P)H quinone dehydrogenase 1 (NQO1), and catalase after treatments. We observed no change in SOD1 and SOD2 expression by either afatinib or palbociclib, while palbociclib increased the SOD3, catalase, and NQO1 levels. Except for SOD3, neither afatinib alone nor in combination with palbociclib could subsequently decrease the expression of these enzymes in the cells (Fig. 4e).

Catalase and NQO1 expression are regulated by transcription factor NRF2. NRF2 is known to interact with KEAP1 to promote polyubiquitination for subsequent proteasomal degradation; however, during increased oxidative stress this interaction is prevented, allowing NRF2 to translocate inside the nucleus and regulate gene expression [43]. Our results showed that combination treatment decreases NRF2 levels to induce ROS production and senescence, and this can be blocked by 15 mM of antioxidant N-acetyl cysteine pretreatment (Fig. 4a & Supplementary Fig. S6a). Overall, these results indicate that the combination induces metabolic alteration by decreasing the ATP pool, reducing anti-oxidant enzymes, and increasing the ROS production to induce senescence.

3.6. Combination treatment delays tumor growth in subcutaneous model

Since combination treatment showed an anti-proliferative effect in HNSCC cell lines, we investigated whether similar effect can be recapitulated in the xenograft mouse model [18]. We observed a significant reduction in tumor growth with combination treatment (Fig. 5a–c). In the combination group, the median tumor weight of UMSCC1 xenografts was lower (144.0 mg) compared to afatinib (429.8 mg), palbociclib (344.0 mg) and vehicle control (991.0 mg). Decreased Ki67 staining was observed in all treated mice (Fig. 5c). Although there was an increased expression of p-EGFR (Tyr-1068) and p-S6 (Ser-235/236) in the

palbociclib group, its expression along with p-Rb (Ser-780) and Ki67 was significantly reduced in the combination groups (Fig. 5c).

3.7. Combination treatment delays tumor progression in the genetically engineered mouse model

EGFR [9] and cyclin D1 [44] overexpression is an early event during HNSCC progression, suggesting that simultaneous inhibition of both the pathways may prevent tumor development. To test this hypothesis, HNSCC GEM model: K14-CreER^{tam};LSL-Kras^{G12D};Trp53^{R172H} mice were injected with tamoxifen to activate Cre recombinase. After 10 days of tamoxifen administration, the mice were treated with vehicle control, afatinib (10 mg/kg/day), palbociclib (50 mg/kg/day), or in combination by oral gavage (Fig. 6a). Combination treatment significantly prevented the development of oral tumors compared to mice treated with single drug or vehicle controls (Fig. 6a). Strikingly, after a gross histological examination of the oral tissues, we found that combination treatment significantly impeded the HNSCC progression with no tumor in 1/5 (20%), dysplastic features in 2/5 (40%) and tumor in 2/5 (40%) in contrast to the presence of squamous cell carcinoma in all single agent or vehicle treated mice (Fig. 6a). Thus, co-targeting EGFR and cyclin D1-CDK4/6 signaling interferes the neoplastic transformation process in HNSCC. At the molecular level, there was a robust decrease in the expression of p-EGFR (Tyr-1068), p-Rb (Ser-780), p-S6 (Ser-235/236), cyclin D1, and CDK4 levels in combination treated mice compared to control or single drug treatments (Fig. 6b).

4. Discussion

Despite significant advances in multimodal therapies, patients with HNSCC develop distant metastases with a dismal prognosis and limited cure. HNSCC is a heterogeneous disease [45] with dysregulated cell cycle and involves overexpression/hyperactivation of EGFR, and cyclin D1-CDK4/6 signaling. EGFR and cyclin D1-CDK4/6 signaling is known to converge at mTOR1-S6K-S6 pathway to modulate cell growth and metabolism [12, 13, 46]. Although EGFR signalling is hyperactivated in HNSCC, targeted therapy has shown limited clinical value with a response rate less than 10% as a monotherapy [47]. One possible mechanism for such dismal response is attributed to the development of intrinsic resistance and simultaneous activation of alternative signaling pathways to overcome tumor cell killing [48]. For example, HNSCC cells treated with gefitinib lead to the subsequent development of acquired resistance via increasing cyclin D1 expression [9]. Similarly, although our previous study with afatinib radio-sensitized the HNSCC cell lines [18]; however, the xenografts that were non-responsive to the treatments showed an increased levels of cyclin D1, CDK4, CDK6, and p-EGFR (Tyr-1068). In breast cancer, increased cyclin D1 expression was associated with resistance to EGFR targeted therapy but can be sensitized by either targeting cyclin D1 or by CDK4/6 inhibitor, abemaciclib [16]. It was noted that targeting CDK4/6 also activated the EGFR signaling to develop resistance to erlotinib in oesophageal cancer [49]. These reports suggested the presence of a feedback loop between EGFR and cyclin D1-CDK4/6 signaling that may result in the development of resistance to monotherapy. Several studies have successfully shown synergistic effect of CDK4/6

inhibitor when combined with other inhibitors that targets AKT, MAPK/ERK or mTOR1 pathway in various types of cancer [50–53].

This study comprehensively evaluated the therapeutic efficacy of afatinib and palbociclib in-combination in the preclinical models to present a strong case for clinical trial in HNSCC. Our results have shown a robust antiproliferative effect during combination treatment both *in vitro* and *in vivo,* and also delayed the tumor progression in the GEM model of HNSCC. At the molecular level, we observed decreased phosphorylation of Rb (Ser-807/811), mTOR1 (Ser-2448), and S6 (Ser-235/236) proteins to cause cell cycle arrest, metabolic alterations, ROS production, and induction of cellular senescence. We also observed that higher cytoplasmic p-S6 expression was associated with shorter disease-free survival in HNSCC patients and may serve as a potential novel biomarker for therapeutic response. The fact that increased p-S6 level was associated with resistance to HER2 and mTOR1 inhibitors in many cancers [35, 54] further highlights its clinical relevance.

Inactivating phosphorylation of Rb by cyclin D1-CDK4/6 complex facilitates the release of E2F necessary for S-phase cell cycle entry; therefore, targeting Rb presents a unique strategy to combat tumor growth in HNSCC. Our results with palbociclib treatment inhibited the phosphorylation of Rb to cause G1 cell cycle arrest of UMSCC1 cells with a concurrent induction of cyclin D1, p-EGFR (Tyr-1068), and p-S6 (Ser-235/236) expression which suggest the existence of resistance to CDK4/6 inhibition. Although reasons for such expression is not well understood, a previous study has shown that inhibiting CDK (activity) activates the TSC2 (inhibitor of mTOR1) to relieve the feedback inhibition upstream of EGFR family kinases [16]. Thus, dual targeting presents a better scenario in such condition; for example, a recent strategy to target cyclin D1 with palbociclib and aromatase inhibitor, letrozole have shown promise in breast cancer [55]. Our present study and previous results [18] have shown afatinib to inhibit EGFR/ERK signalling and decrease the cyclin D1 expression resulting in G1 arrest, inhibition of cell proliferation, and potentially prevent resistance development. Activation of EGFR/mTOR1/P70-S6K/S6 signaling in the cancer cells provides a cellular advantage to survive and grow through metabolic reprogramming [12, 13, 46]. Our results showed that palbociclib induced the mTOR1/S6 phosphorylation to increase cell metabolism and ATP generation, thus may present treatment liability as a monotherapy. Therefore, combining palbociclib with afatinib not only decreases the ATP levels, but also concurrently decreased the glycolysis and TCA cycle intermediates. However, the contrasting outcome of CDK4/6 inhibitor in-combination with other inhibitors still exist. Synergistic effects of CDK4/6 inhibitor along with MEK/mTOR1 or PI3K inhibition was observed in pancreatic [36] and breast cancer [56], while there was no synergy between PI3K and CDK4/6 inhibitors in the pancreatic cancer cells [36].

Therapy-induced senescence (TIS) is a novel approach to induce cytostasis in tumor cells. EGFR [34] and CDK4/6 [57] inhibition is shown to cause cell cycle arrest and induce cellular senescence by ROS production. Low cellular energy and mitochondrial dysfunction are other factors associated with the TIS [57]. Our results with palbociclib and afatinib treatments could induce the cell cycle arrest, senescence, and ROS production; this effect was further enhanced when used in-combination suggesting its dual targeting effectiveness. The cellular antioxidant system, including NRF2, KEAP1, catalase, HO1, SODs, etc., are

deregulated in many cancers and modulate the cellular ROS levels; this system has been exploited to promote cell death or cell cycle arrest in many cancers [58]. Our study showed that afatinib treatment downregulated the expression of SOD3, NQO1, NRF2, and catalase, thereby contributing to the enhanced palbociclib-induced ROS generation and senescence, and subsequently suppressed the tumor growth. Furthermore, afatinib treatment restricted the cancer cells from entry into glycolysis and TCA cycle induced by the palbociclib. CDK4/6 is known to stabilize and activate the transcription factor Forkhead Box M1 (FOXM1) to regulate the expression of G1/S cell cycle genes and suppress ROS production to protect the cells from senescence [57]. We also observed a drastic reduction of FOXM1 expression during combination treatment suggesting its role in the increased redox signaling to induce senescence in HNSCC.

As EGFR/mTOR1 and cyclin D1 pathways are frequently dysregulated in the early dysplastic lesions and invasive HNSCC tumors [4, 5, 44, 59] in-addition to recurrent tumors; targeting these pathways may potentially reduce the tumor growth, disease progression, resistance development, and tumor recurrence via preventing the feedback regulation. Our data clearly showed that co-targeting EGFR and CDK4/6 could significantly inhibit tumor growth in both the mouse models. Finally, we noted that the combination treatment in our GEM model prevented the development of frank malignancy in 60% of mice and restricted the tumor growth at dysplastic lesions. We speculate that improvement in such partial response (enhanced antitumor activity) can be achieved by exploring the time- and dose escalation studies for this combination.

In summary, this study indicates the presence of alternative pathways in the EGFR and cyclin D1 overexpressed HNSCC patients that evade traditional treatment strategies to promote cancer cell proliferation and survival. Therefore, simultaneous inhibition of these pathways by afatinib and palbociclib potentiates the combined anti-tumor effects in both the *in vitro* and *in vivo* models via metabolic disruption, ROS scavenging mechanisms, and cell cycle progression (Fig. 6b). Overall, this study provides a strong rationale for clinical evaluation of combination therapy in HNSCC patients.

Supplementary Material

Refer to Web version on PubMed Central for supplementary material.

Acknowledgments

The authors/work in the manuscript are supported, in part, by the grants from the National Institutes of Health (P01 CA217798, R01 CA195586, R01 CA 210637, R01 CA247471, R01 CA 206444, R01CA218545, and R01CA241752) and Veteran Affairs (I01 BX004676). Dr. Macha is a recipient of Ramalingaswami Fellowship (D.O.NO.BT/HRD/35/02/2006) from the Department of Biotechnology, Govt. of India, New Delhi, India. We thank Janice A. Taylor and James R. Talaska for technical assistance in confocal laser scanning microscope, Victoria B. Smith and Samantha D. Wall for flow cytometry experiments. We also thank the Boston University Metabolomics service Center for the metabolite analysis.

References

[1]. Sigismund S, Avanzato D, Lanzetti L, Emerging functions of the EGFR in cancer, Molecular oncology, 12 (2018) 3–20. [PubMed: 29124875]

[2]. Sasaki T, Hiroki K, Yamashita Y, The role of epidermal growth factor receptor in cancer metastasis and microenvironment, Biomed Res Int, 2013 (2013) 546318. [PubMed: 23986907]

[3]. Macha MA, Rachagani S, Chaudhary S, Sayed Z, Jones DT, Batra SK, Receptor Tyrosine Kinase Signaling Pathways as a Goldmine for Targeted Therapy in Head and Neck Cancers, Gene Regulation and Therapeutics for Cancer, 163.

[4]. Chaudhary S, Dam V, Ganguly K, Sharma S, Atri P, Chirravuri-Venkata R, Cox JL, Sayed Z, Jones DT, Ganti AK, Ghersi D, Macha MA, Batra SK, Differential mutation spectrum and immune landscape in African Americans versus Whites: A possible determinant to health disparity in head and neck cancer, Cancer Letters, 492 (2020) 44–53. [PubMed: 32738272]

[5]. Alao JP, The regulation of cyclin D1 degradation: roles in cancer development and the potential for therapeutic invention, Molecular cancer, 6 (2007) 24. [PubMed: 17407548]

[6]. Yu Z, Weinberger PM, Haffty BG, Sasaki C, Zerillo C, Joe J, Kowalski D, Dziura J, Camp RL, Rimm DL, Cyclin d1 is a valuable prognostic marker in oropharyngeal squamous cell carcinoma, Clinical cancer research, 11 (2005) 1160–1166. [PubMed: 15709184]

[7]. Inoue K, Fry EA, Aberrant expression of p16INK4a in human cancers–a new biomarker?, Cancer reports and reviews, 2 (2018).

[8]. Khan H, Gupta S, Husain N, Misra S, Negi M, Jamal N, Ghatak A, Correlation between expressions of Cyclin-D1, EGFR and p53 with chemoradiation response in patients of locally advanced oral squamous cell carcinoma, BBA clinical, 3 (2015) 11–17. [PubMed: 26675419]

[9]. Kalish LH, Kwong RA, Cole IE, Gallagher RM, Sutherland RL, Musgrove EA, Deregulated cyclin D1 expression is associated with decreased efficacy of the selective epidermal growth factor receptor tyrosine kinase inhibitor gefitinib in head and neck squamous cell carcinoma cell lines, Clinical cancer research, 10 (2004) 7764–7774. [PubMed: 15570011]

[10]. Cohen EEW, Bell RB, Bifulco CB, Burtness B, Gillison ML, Harrington KJ, Le QT, Lee NY, Leidner R, Lewis RL, Licitra L, Mehanna H, Mell LK, Raben A, Sikora AG, Uppaluri R, Whitworth F, Zandberg DP, Ferris RL, The Society for Immunotherapy of Cancer consensus statement on immunotherapy for the treatment of squamous cell carcinoma of the head and neck (HNSCC), J Immunother Cancer, 7 (2019) 184. [PubMed: 31307547]

[11]. Chaudhary S, Ganguly K, Muniyan S, Pothuraju R, Sayed Z, Jones DT, Batra SK, Macha MA, Immunometabolic alterations by HPV infection: new dimensions to head and neck cancer disparity, JNCI: Journal of the National Cancer Institute, 111 (2019) 233–244. [PubMed: 30615137]

[12]. Musgrove EA, Caldon CE, Barraclough J, Stone A, Sutherland RL, Cyclin D as a therapeutic target in cancer, Nature Reviews Cancer, 11 (2011) 558–572. [PubMed: 21734724]

[13]. Kaplon J, van Dam L, Peeper D, Two-way communication between the metabolic and cell cycle machineries: the molecular basis, Cell Cycle, 14 (2015) 2022–2032. [PubMed: 26038996]

[14]. Jin N, Bi A, Lan X, Xu J, Wang X, Liu Y, Wang T, Tang S, Zeng H, Chen Z, Tan M, Ai J, Xie H, Zhang T, Liu D, Huang R, Song Y, Leung EL-H, Yao X, Ding J, Geng M, Lin S-H, Huang M, Identification of metabolic vulnerabilities of receptor tyrosine kinases-driven cancer, Nature Communications, 10 (2019) 2701.

[15]. Lim AM, Do H, Young RJ, Wong SQ, Angel C, Collins M, Takano EA, Corry J, Wiesenfeld D, Kleid S, Differential mechanisms of CDKN2A (p16) alteration in oral tongue squamous cell carcinomas and correlation with patient outcome, International journal of cancer, 135 (2014) 887–895. [PubMed: 24436120]

[16]. Goel S, Wang Q, Watt AC, Tolaney SM, Dillon DA, Li W, Ramm S, Palmer AC, Yuzugullu H, Varadan V, Tuck D, Harris LN, Wong K-K, Liu XS, Sicinski P, Winer EP, Krop IE, Zhao JJ, Overcoming Therapeutic Resistance in HER2-Positive Breast Cancers with CDK4/6 Inhibitors, Cancer cell, 29 (2016) 255–269. [PubMed: 26977878]

[17]. Byeon HK, Ku M, Yang J, Beyond EGFR inhibition: multilateral combat strategies to stop the progression of head and neck cancer, Experimental & Molecular Medicine, 51 (2019) 1–14.

[18]. Macha MA, Rachagani S, Qazi AK, Jahan R, Gupta S, Patel A, Seshacharyulu P, Lin C, Li S, Wang S, Verma V, Kishida S, Kishida M, Nakamura N, Kibe T, Lydiatt WM, Smith RB, Ganti AK, Jones DT, Batra SK, Jain M, Afatinib radiosensitizes head and neck squamous cell

carcinoma cells by targeting cancer stem cells, Oncotarget, 8 (2017) 20961–20973. [PubMed: 28423495]

[19]. Klein ME, Kovatcheva M, Davis LE, Tap WD, Koff A, CDK4/6 Inhibitors: The Mechanism of Action May Not Be as Simple as Once Thought, Cancer Cell, 34 (2018) 9–20. [PubMed: 29731395]

[20]. Orcutt KP, Parsons AD, Sibenaller ZA, Scarbrough PM, Zhu Y, Sobhakumari A, Wilke WW, Kalen AL, Goswami P, Miller FJ Jr., Spitz DR, Simons AL, Erlotinib-mediated inhibition of EGFR signaling induces metabolic oxidative stress through NOX4, Cancer Res, 71 (2011) 3932–3940. [PubMed: 21482679]

[21]. Pothuraju R, Rachagani S, Krishn SR, Chaudhary S, Nimmakayala RK, Siddiqui JA, Ganguly K, Lakshmanan I, Cox JL, Mallya K, Kaur S, Batra SK, Molecular implications of MUC5AC-CD44 axis in colorectal cancer progression and chemoresistance, Molecular Cancer, 19 (2020) 37. [PubMed: 32098629]

[22]. Chatterjee S, Malhotra R, Varghese F, Bukhari AB, Patil A, Budrukkar A, Parmar V, Gupta S, De A, Quantitative immunohistochemical analysis reveals association between sodium iodide symporter and estrogen receptor expression in breast cancer, PLoS One, 8 (2013) e54055. [PubMed: 23342072]

[23]. Chaudhary S, Madhukrishna B, Adhya AK, Keshari S, Mishra SK, Overexpression of caspase 7 is ERα dependent to affect proliferation and cell growth in breast cancer cells by targeting p21Cip, Oncogenesis, 5 (2016) e219–e219. [PubMed: 27089142]

[24]. Ianevski A, Giri AK, Aittokallio T, SynergyFinder 2.0: visual analytics of multi-drug combination synergies, Nucleic Acids Research, 48 (2020) W488–W493. [PubMed: 32246720]

[25]. Debacq-Chainiaux F, Erusalimsky JD, Campisi J, Toussaint O, Protocols to detect senescence-associated beta-galactosidase (SA-betagal) activity, a biomarker of senescent cells in culture and in vivo, Nat Protoc, 4 (2009) 1798–1806. [PubMed: 20010931]

[26]. Shukla SK, Purohit V, Mehla K, Gunda V, Chaika NV, Vernucci E, King RJ, Abrego J, Goode GD, Dasgupta A, Illies AL, Gebregiworgis T, Dai B, Augustine JJ, Murthy D, Attri KS, Mashadova O, Grandgenett PM, Powers R, Ly QP, Lazenby AJ, Grem JL, Yu F, Matés JM, Asara JM, Kim JW, Hankins JH, Weekes C, Hollingsworth MA, Serkova NJ, Sasson AR, Fleming JB, Oliveto JM, Lyssiotis CA, Cantley LC, Berim L, Singh PK, MUC1 and HIF-1alpha Signaling Crosstalk Induces Anabolic Glucose Metabolism to Impart Gemcitabine Resistance to Pancreatic Cancer, Cancer Cell, 32 (2017) 71–87.e77. [PubMed: 28697344]

[27]. Macha MA, Rachagani S, Pai P, Gupta S, Lydiatt WM, Smith RB, Johansson SL, Lele SM, Kakar SS, Lee JH, Meza J, Ganti AK, Jain M, Batra SK, MUC4 regulates cellular senescence in head and neck squamous cell carcinoma through p16/Rb pathway, Oncogene, 34 (2015) 1698–1708. [PubMed: 24747969]

[28]. Raimondi AR, Molinolo A, Gutkind JS, Rapamycin prevents early onset of tumorigenesis in an oral-specific K-ras and p53 two-hit carcinogenesis model, Cancer Res, 69 (2009) 4159–4166. [PubMed: 19435901]

[29]. Ang KK, Berkey BA, Tu X, Zhang HZ, Katz R, Hammond EH, Fu KK, Milas L, Impact of epidermal growth factor receptor expression on survival and pattern of relapse in patients with advanced head and neck carcinoma, Cancer Res, 62 (2002) 7350–7356. [PubMed: 12499279]

[30]. Picon H, Guddati AK, Mechanisms of resistance in head and neck cancer, Am J Cancer Res, 10 (2020) 2742–2751. [PubMed: 33042614]

[31]. Ruvinsky I, Meyuhas O, Ribosomal protein S6 phosphorylation: from protein synthesis to cell size, Trends Biochem Sci, 31 (2006) 342–348. [PubMed: 16679021]

[32]. Kim SH, Jang YH, Chau GC, Pyo S, Um SH, Prognostic significance and function of phosphorylated ribosomal protein S6 in esophageal squamous cell carcinoma, Mod Pathol, 26 (2013) 327–335. [PubMed: 22996377]

[33]. Katholnig K, Schütz B, Fritsch SD, Schörghofer D, Linke M, Sukhbaatar N, Matschinger JM, Unterleuthner D, Hirtl M, Lang M, Herac M, Spittler A, Bergthaler A, Schabbauer G, Bergmann M, Dolznig H, Hengstschläger M, Magnuson MA, Mikula M, Weichhart T, Inactivation of mTORC2 in macrophages is a signature of colorectal cancer that promotes tumorigenesis, JCI Insight, 4 (2019).

[34]. Alexander PB, Yuan L, Yang P, Sun T, Chen R, Xiang H, Chen J, Wu H, Radiloff DR, Wang X-F, EGF promotes mammalian cell growth by suppressing cellular senescence, Cell Research, 25 (2015) 135–138. [PubMed: 25367123]

[35]. Iwenofu OH, Lackman RD, Staddon AP, Goodwin DG, Haupt HM, Brooks JSJ, Phospho-S6 ribosomal protein: a potential new predictive sarcoma marker for targeted mTOR therapy, Modern Pathology, 21 (2008) 231–237. [PubMed: 18157089]

[36]. Franco J, Balaji U, Freinkman E, Witkiewicz AK, Knudsen ES, Metabolic Reprogramming of Pancreatic Cancer Mediated by CDK4/6 Inhibition Elicits Unique Vulnerabilities, Cell Rep, 14 (2016) 979–990. [PubMed: 26804906]

[37]. Voronina SG, Barrow SL, Simpson AW, Gerasimenko OV, da Silva Xavier G, Rutter GA, Petersen OH, Tepikin AV, Dynamic changes in cytosolic and mitochondrial ATP levels in pancreatic acinar cells, Gastroenterology, 138 (2010) 1976–1987. [PubMed: 20102715]

[38]. Bonora M, Patergnani S, Rimessi A, De Marchi E, Suski JM, Bononi A, Giorgi C, Marchi S, Missiroli S, Poletti F, Wieckowski MR, Pinton P, ATP synthesis and storage, Purinergic Signal, 8 (2012) 343–357. [PubMed: 22528680]

[39]. Veitia RA, DNA Content, Cell Size, and Cell Senescence, Trends Biochem Sci, 44 (2019) 645–647. [PubMed: 31160123]

[40]. Neurohr GE, Terry RL, Lengefeld J, Bonney M, Brittingham GP, Moretto F, Miettinen TP, Vaites LP, Soares LM, Paulo JA, Harper JW, Buratowski S, Manalis S, van Werven FJ, Holt LJ, Amon A, Excessive Cell Growth Causes Cytoplasm Dilution And Contributes to Senescence, Cell, 176 (2019) 1083–1097.e1018. [PubMed: 30739799]

[41]. Liemburg-Apers DC, Willems PH, Koopman WJ, Grefte S, Interactions between mitochondrial reactive oxygen species and cellular glucose metabolism, Arch Toxicol, 89 (2015) 1209–1226. [PubMed: 26047665]

[42]. Galloway CA, Yoon Y, Perspectives on: SGP symposium on mitochondrial physiology and medicine: what comes first, misshape or dysfunction? The view from metabolic excess, J Gen Physiol, 139 (2012) 455–463. [PubMed: 22641640]

[43]. Chio IIC, Tuveson DA, ROS in Cancer: The Burning Question, Trends Mol Med, 23 (2017) 411–429. [PubMed: 28427863]

[44]. Ramakrishna A, Shreedhar B, Narayan T, Mohanty L, Shenoy S, Jamadar S, Cyclin D1 an early biomarker in oral carcinogenesis, J Oral Maxillofac Pathol, 17 (2013) 351–357. [PubMed: 24574651]

[45]. Canning M, Guo G, Yu M, Myint C, Groves MW, Byrd JK, Cui Y, Heterogeneity of the Head and Neck Squamous Cell Carcinoma Immune Landscape and Its Impact on Immunotherapy, Front Cell Dev Biol, 7 (2019) 52. [PubMed: 31024913]

[46]. Asghar U, Witkiewicz AK, Turner NC, Knudsen ES, The history and future of targeting cyclin-dependent kinases in cancer therapy, Nature Reviews Drug Discovery, 14 (2015) 130–146. [PubMed: 25633797]

[47]. Bernier J, Bentzen SM, Vermorken JB, Molecular therapy in head and neck oncology, Nat Rev Clin Oncol, 6 (2009) 266–277. [PubMed: 19390553]

[48]. Alsahafi E, Begg K, Amelio I, Raulf N, Lucarelli P, Sauter T, Tavassoli M, Clinical update on head and neck cancer: molecular biology and ongoing challenges, Cell Death & Disease, 10 (2019) 540. [PubMed: 31308358]

[49]. Zhou J, Wu Z, Wong G, Pectasides E, Nagaraja A, Stachler M, Zhang H, Chen T, Zhang H, Liu JB, Xu X, Sicinska E, Sanchez-Vega F, Rustgi AK, Diehl JA, Wong K-K, Bass AJ, CDK4/6 or MAPK blockade enhances efficacy of EGFR inhibition in oesophageal squamous cell carcinoma, Nature Communications, 8 (2017) 13897.

[50]. Cretella D, Ravelli A, Fumarola C, La Monica S, Digiacomo G, Cavazzoni A, Alfieri R, Biondi A, Generali D, Bonelli M, Petronini PG, The anti-tumor efficacy of CDK4/6 inhibition is enhanced by the combination with PI3K/AKT/mTOR inhibitors through impairment of glucose metabolism in TNBC cells, J Exp Clin Cancer Res, 37 (2018) 72. [PubMed: 29587820]

[51]. Lee MS, Helms TL, Feng N, Gay J, Chang QE, Tian F, Wu JY, Toniatti C, Heffernan TP, Powis G, Kwong LN, Kopetz S, Efficacy of the combination of MEK and CDK4/6 inhibitors in vitro

and in vivo in KRAS mutant colorectal cancer models, Oncotarget, 7 (2016) 39595–39608. [PubMed: 27167191]

[52]. Liu M, Xu S, Wang Y, Li Y, Li Y, Zhang H, Liu H, Chen J, PD 0332991, a selective cyclin D kinase 4/6 inhibitor, sensitizes lung cancer cells to treatment with epidermal growth factor receptor tyrosine kinase inhibitors, Oncotarget, 7 (2016) 84951–84964. [PubMed: 27825114]

[53]. Liu S, Tang Y, Yuan X, Yuan D, Liu J, Li B, Li Y, Inhibition of Rb and mTOR signaling associates with synergistic anticancer effect of palbociclib and erlotinib in glioblastoma cells, Invest New Drugs, 36 (2018) 961–969. [PubMed: 29508248]

[54]. Yang-Kolodji G, Mumenthaler SM, Mehta A, Ji L, Tripathy D, Phosphorylated ribosomal S6 (p-rpS6) as a post-treatment indicator of HER2 signalling targeted drug resistance, Biomarkers, 20 (2015) 313–322. [PubMed: 26329528]

[55]. Sherr CJ, Beach D, Shapiro GI, Targeting CDK4 and CDK6: From Discovery to Therapy, Cancer Discov, 6 (2016) 353–367. [PubMed: 26658964]

[56]. Vora SR, Juric D, Kim N, Mino-Kenudson M, Huynh T, Costa C, Lockerman EL, Pollack SF, Liu M, Li X, Lehar J, Wiesmann M, Wartmann M, Chen Y, Cao ZA, Pinzon-Ortiz M, Kim S, Schlegel R, Huang A, Engelman JA, CDK 4/6 inhibitors sensitize PIK3CA mutant breast cancer to PI3K inhibitors, Cancer Cell, 26 (2014) 136–149. [PubMed: 25002028]

[57]. Anders L, Ke N, Hydbring P, Choi YJ, Widlund HR, Chick JM, Zhai H, Vidal M, Gygi SP, Braun P, Sicinski P, A systematic screen for CDK4/6 substrates links FOXM1 phosphorylation to senescence suppression in cancer cells, Cancer Cell, 20 (2011) 620–634. [PubMed: 22094256]

[58]. Gorrini C, Harris IS, Mak TW, Modulation of oxidative stress as an anticancer strategy, Nat Rev Drug Discov, 12 (2013) 931–947. [PubMed: 24287781]

[59]. Harari PM, Wheeler DL, Grandis JR, Molecular target approaches in head and neck cancer: epidermal growth factor receptor and beyond, Semin Radiat Oncol, 19 (2009) 63–68. [PubMed: 19028347]

- Hyperactive EGFR and cyclin D1-CDK4/6 activates alternative pathway to induce therapy resistance.
- Phosphorylated S6, downstream effector molecule of EGFR and cyclin D1-CDK4/6 signalling may serve as prognostic marker.
- Combination treatments with afatinib and palbociclib showed robust cytostatic effect, decreased metabolism, and cellular senescence.
- Combination therapy reduced or delayed tumor progression in the mouse models.

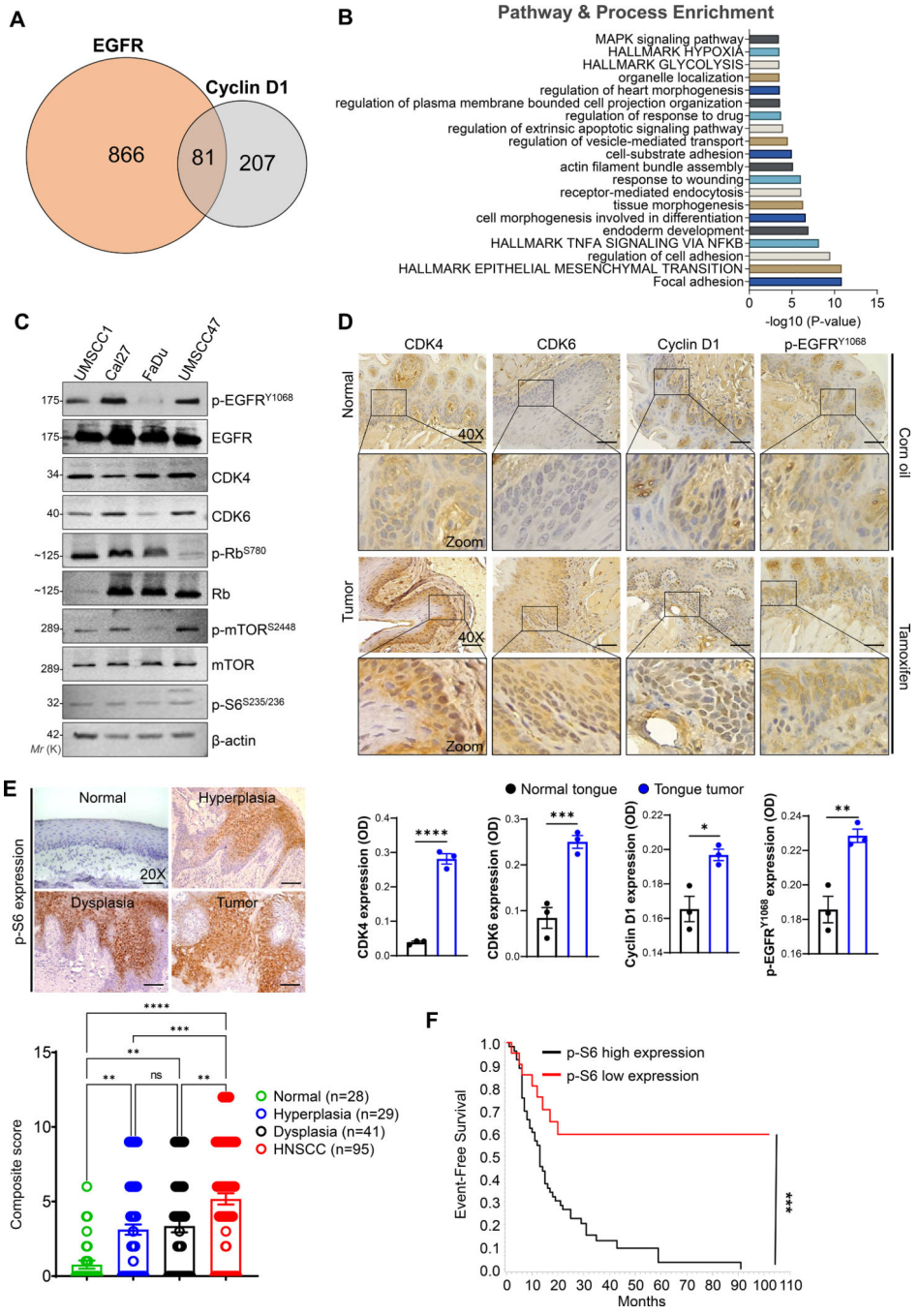

Fig. 1. Hyperactivation of EGFR and cyclin D1-CDK4/6 signaling in HNSCC.

a. Venn diagram showing co-expressed genes with EGFR (947 genes) and cyclin D1 (288 genes) in TCGA HNSCC patients extracted from the cBioPortal (https://www.cbioportal.org/). Eighty-one genes are common across the two gene sets. **b**. Gene set enrichment analysis (https://metascape.org/gp/) based on pathway and processes indicate the gene clusters associated with EGFR and cyclin D1 in regulating the hallmarks of glycolysis, epithelial to mesenchymal transition, and cell growth, etc., **c.** Western blot analysis of EGFR and CDK4/6 signaling proteins in whole cell lysates (20–40 μg) loaded in 8–12 % SDS-

PAGE. β-actin used as a loading control. **d.** Immunohistochemistry in normal (corn oil injected) and tumor tissues (tamoxifen injected) obtained from the genetically engineered mice model (K14-CreER^{tam};LSL-Kras^{G12D};Trp53^{R172H}). Representative immunohistochemistry images were photographed by Leica ICC50E (40X). p-EGFR (Tyr-1068), cyclin D1, CDK4, and CDK6 was analyzed in the tissues (n=3) using ImageJ (IHC Profiler plugin) [22]. The quantification of positive staining (OD) of the respective proteins are provided (bottom panel). Optical density (OD) = log (max density/mean intensity). e, f. Representative immunohistochemistry images of p-S6 (Ser-235/236) analyzed in normal (n=28), leukoplakia (n=70) [hyperplasia (n=29), dysplasia (n=41)], and HNSCC (n=95)]. Staining represented as a composite score [intensity score × percentage positive cells]. Event-free survival of HNSCC patients based on p-S6 expression. Data represent mean ± SEM. Unpaired two-tailed *t*-test **(d & f)** and Ordinary one-way ANOVA with Tukey's multiple comparisons test **(e)**. **P < 0.01, ***P < 0.001, ****P < 0.0001, and ns=non-significant.

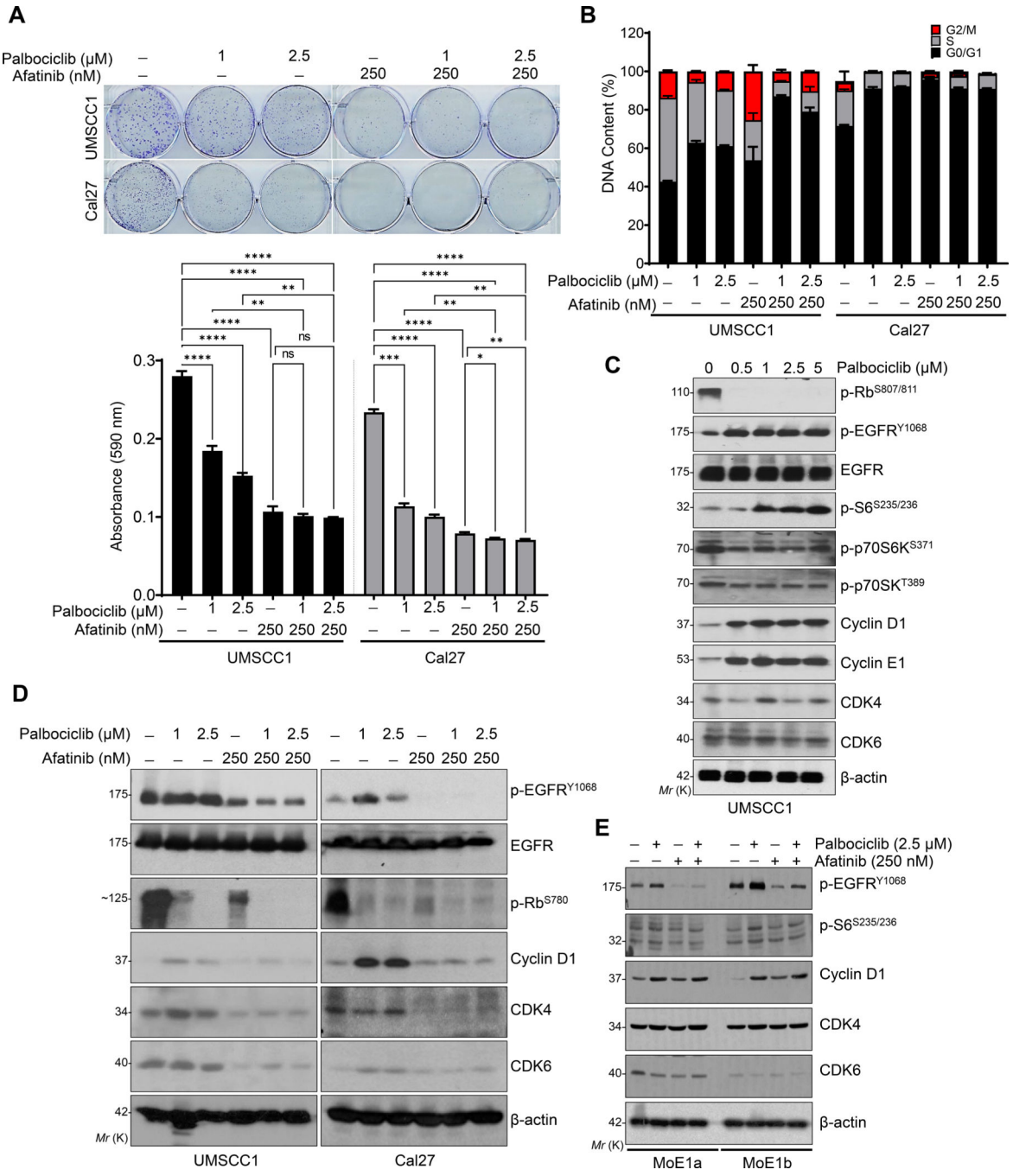

Fig. 2. Afatinib and palbociclib in-combination decrease the proliferation of HNSCC cells by inducing cell cycle arrest.

a. Representative images of colony formation assay after 15–21 days of treatments with palbociclib (1 and 2.5 μM), afatinib (250 nM) or combination (palbociclib- 1 & 2.5 μM and afatinib- 250 nM) in UMSCC1 and Cal27 cell lines. Quantification was performed (absorbance at 590 nm) after dissolving the colonies (0.5% crystal violet staining) with 10% acetic acid and represented as bar diagram (bottom panel). **b.** Distribution of DNA content (in percentage) by Flow cytometry analysis (UMSCC1 and Cal27) after palbociclib (1 and

2.5 μM), afatinib (250 nM) and combination treatments for 48 h. **c.** Western blot of p-Rb (Ser-807/811), p-EGFR (Tyr-1068), p-S6 (Ser-235/236) and cyclin D1 in the whole cell lysates after dose-dependent treatment with palbociclib (0.5 μM to 5 μM) for 48 h. **d.** Western blot in whole cell lysates after various treatments [palbociclib (1 & 2.5 μM), afatinib (250nM) and combination (palbociclib- 1 & 2.5 μM and afatinib- 250 nM) for 48 h in UMSCC1 and Cal27. Combination treatment affects p-EGFR (Tyr-1068), p-S6 (Ser-235/236), cyclin D1, CDK4, and CDK6 expression. **e**. Western blot after treatments as described (**d**), after 48 h treatment in the immortalized normal oral epithelial cell lines, MoE1a and MoE1b. β-actin as a loading control. Data represent mean ± SEM (n=3). One-way ANOVA and Tukey's multiple comparisons test (**a**). *P < 0.05, **P < 0.01, ***P < 0.001, ****P < 0.0001, and ns=non-significant.

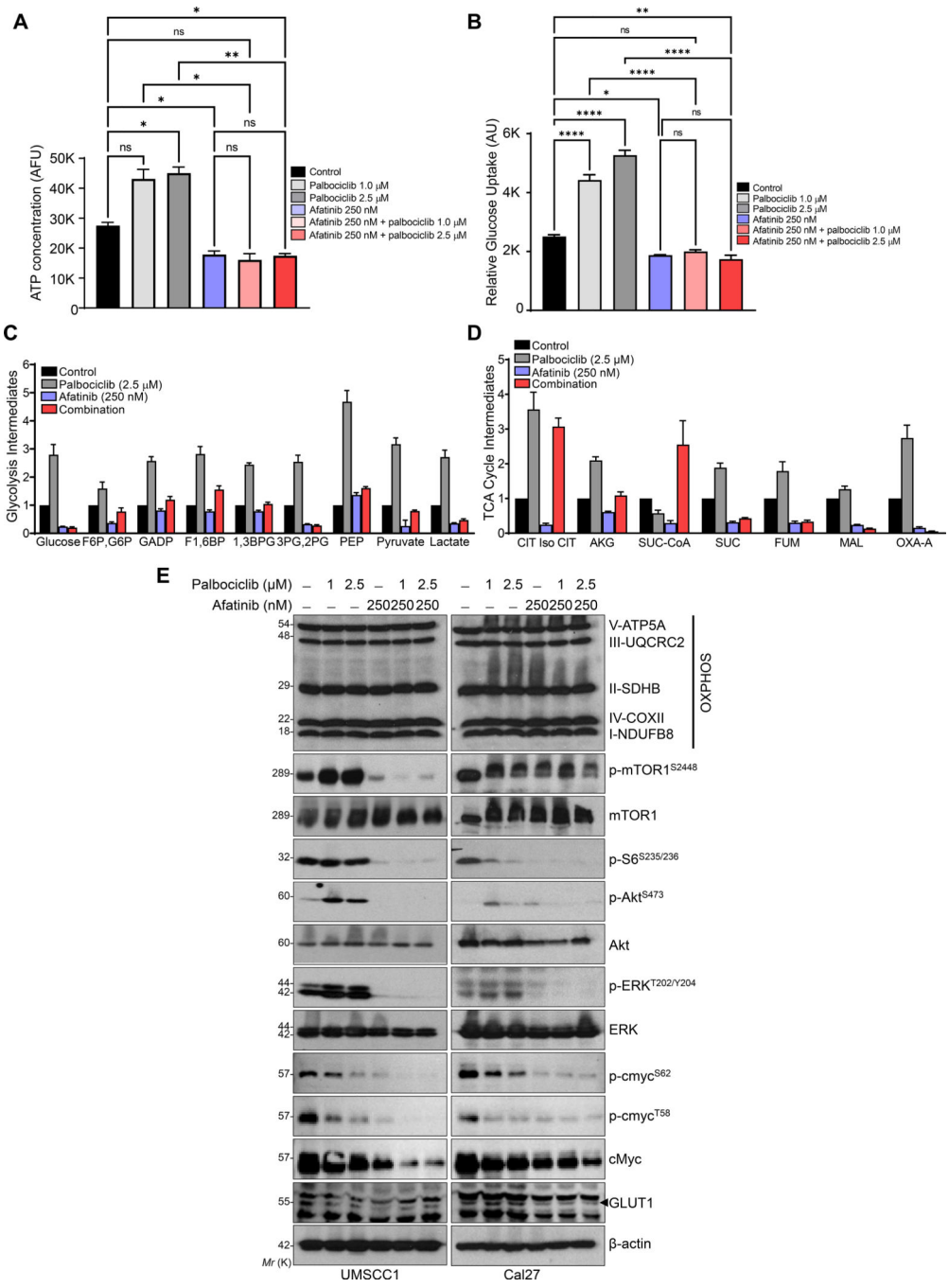

Fig. 3. Combination treatment induces metabolic alteration in HNSCC.

a. UMSCC1 cell line treated with palbociclib (1 & 2.5 μM), afatinib (250 nM) and combination (palbociclib- 1 & 2.5 μM and afatinib- 250 nM) for 48 h. Cellular ATP measured with ATP Detection Assay Kit-Luminescence kit and concentration represented as bar diagram. **b.** Relative glucose uptake measured with Glucose Uptake Cell-Based Assay Kit after treatments described in (**a**). **c, d.** Glycolysis and Tricarboxylic acid cycle (TCA cycle) intermediates were measured by Mass spectrometry after 48 h of treatment [afatinib-250 nm, palbociclib-2.5 μM, and combination (afatinib-250 nm & palbociclib-2.5

μM)] in UMSCC1 cells. Data represented as relative fold change of intermediates in glycolysis: glucose, glucose 6P (G6P), fructose 1,6BP (F6P), Glyceraldehyde 3-phosphate (GADP), Fructose 1,6-bisphosphate (F1,6BP), 1,3-Bisphosphoglycerate (1,3BPG), Glyceraldehyde 3-phosphate (3PG), 2-phosphoglycerate (2PG), Phosphoenolpyruvate (PEP), pyruvate, and lactate; and TCA cycle: Citrate, Iso-citrate (CIT Iso CIT), alpha-ketoglutarate (AKG), Succinyl Co-A (Suc-CoA), Succinate (SUC), fumarate (FUM), malate (MAL), and Oxaloacetate-A (OXA-A). **e**. Western blot in whole cell lysates showing OXPHOS/electron transport chain proteins, p-mTOR1 (Ser-2448), p-AKT (Ser-473), p-ERK (Thr-202/Tyr-204) after treatments as described (**a**) in UMSCC1 and Cal27. β-actin as a loading control. Data represent mean ± SEM. ANOVA followed by Tukey's multiple comparisons test (**a & b**). Statistical significance *P < 0.05, **P < 0.01, ****P < 0.001, and ns=non-significant.

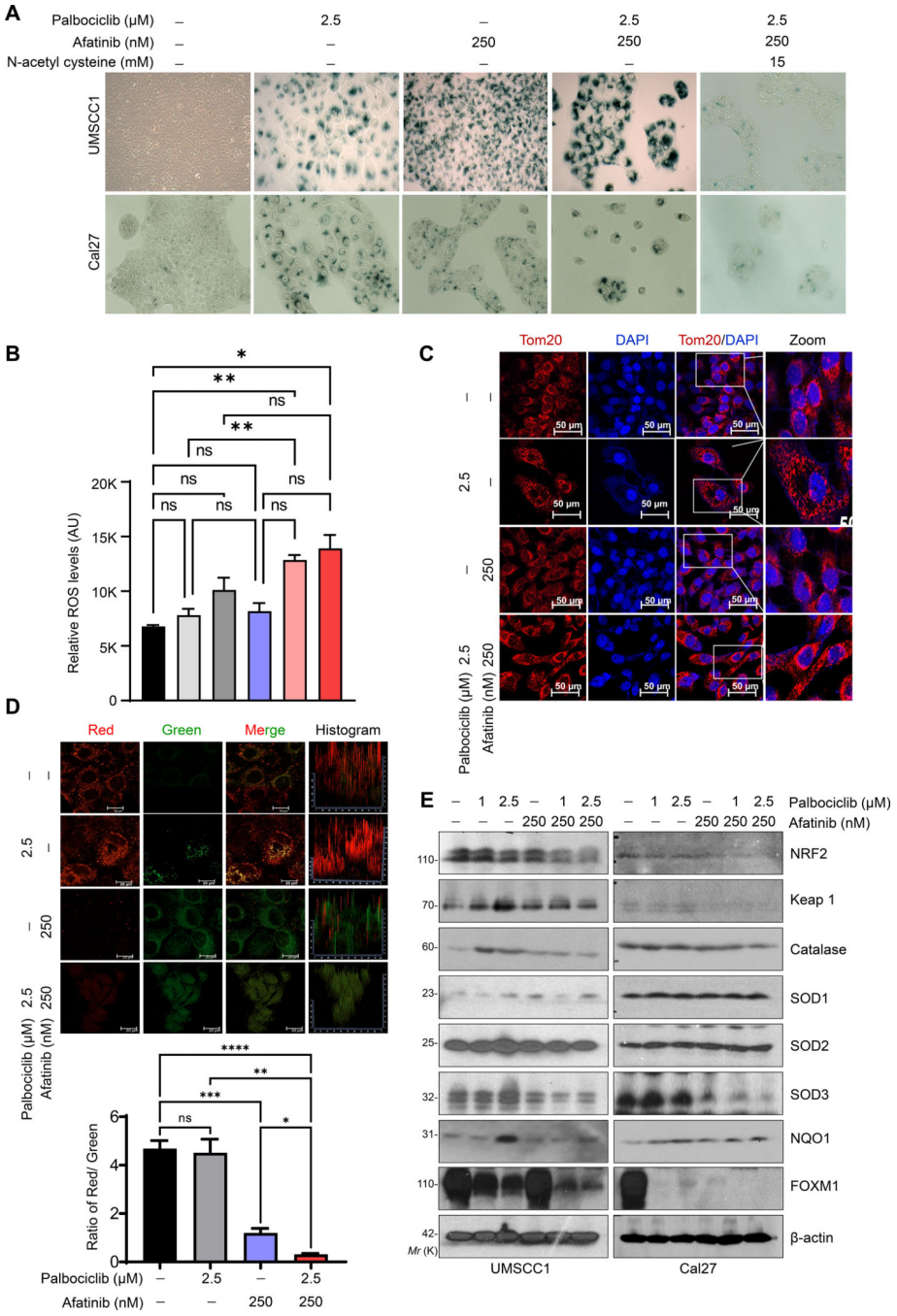

Fig. 4. Combination treatment induces senescence through ROS generation in HNSCC.

a. Representative image of SA-β-gal staining indicates cell senescence in UMSCC1 and Cal27 cells after palbociclib (2.5 μM), afatinib (250 nM) or combination (palbociclib- 2.5 μM and afatinib- 250 nM) for 48 h. Treatment with N-acetyl cysteine (15 mM) for 2–4 h prior to combination treatment (right panel). **b**. Intracellular levels of reactive oxygen species (ROS) measured with Fluorometric Intracellular Ros Kit after 48 h of treatment [palbociclib (1 & 2.5 μM), afatinib (250 nM) and combination (palbociclib- 1 & 2.5 μM and afatinib- 250 nM)]. **c.** Immunofluorescence of mitochondrial Tom20 staining in UMSCC1

after treatment [afatinib-250 nm, palbociclib-2.5 μM, and combination (afatinib-250 nm & palbociclib-2.5 μM)] for 48 h. **d**. Active mitochondria as shown by JC-1 red/green staining. Quantification of ratio of red/green (bottom panel). **e**. Western blot of ROS scavenging proteins after treatment described (**b**) in UMSCC1 and Cal27. Data represent mean ± SEM. n=2. ANOVA followed by Tukey's multiple comparisons test between groups (**b** & **d**). *P < 0.05, **P < 0.01, ***P < 0.001, ****P < 0.0001, and ns=non-significant.

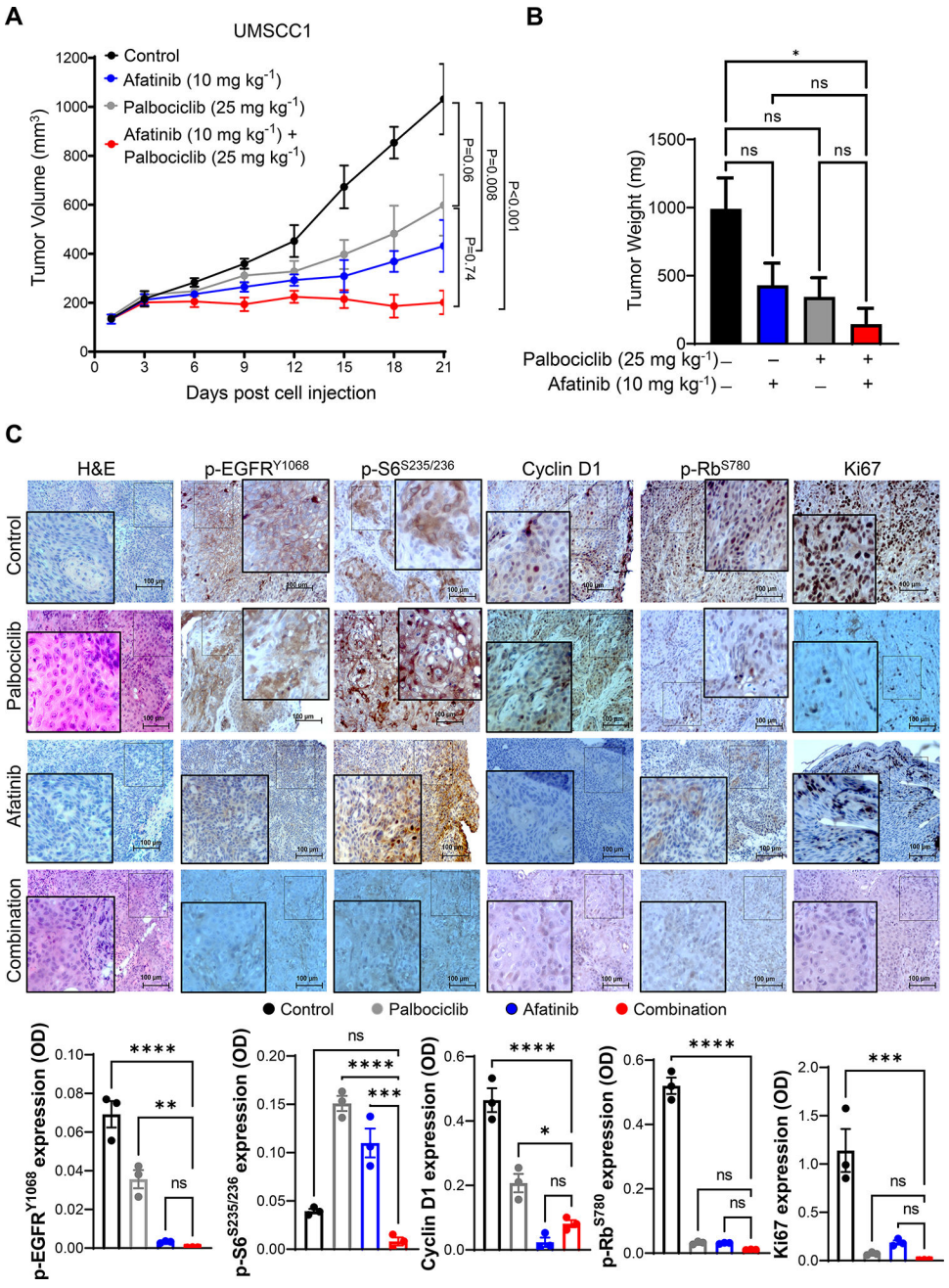

Fig. 5. Combination therapy decreases the growth of HNSCC xenografts.

a. Tumor volume and weight of UMSCC1 xenograft after treatments with afatinib (10 mg/kg/day), palbociclib (25 mg/kg/day), and combination or vehicle for 21 days. Data represent mean tumor volume ± SEM. n=5 mice/group. **b.** Tumor weights of UMSCC1 xenografts (four groups) in milligrams after treatments. **c.** Representative immunohistochemistry image of p-EGFR (Tyr-1068), p-S6 (Ser-235/236), cyclin D1, p-Rb (Ser-780), and Ki67 of xenografts (n=3). Image scale = 100 μm. IHC quantifications (OD) are provided in the bottom panel. Data represent mean ± SEM. ANOVA followed by

Tukey's multiple comparisons test was used between groups (**a-c**). *P < 0.05, **P < 0.01, ***P < 0.001, ****P < 0.0001, and ns=non-significant. OD=optical density.

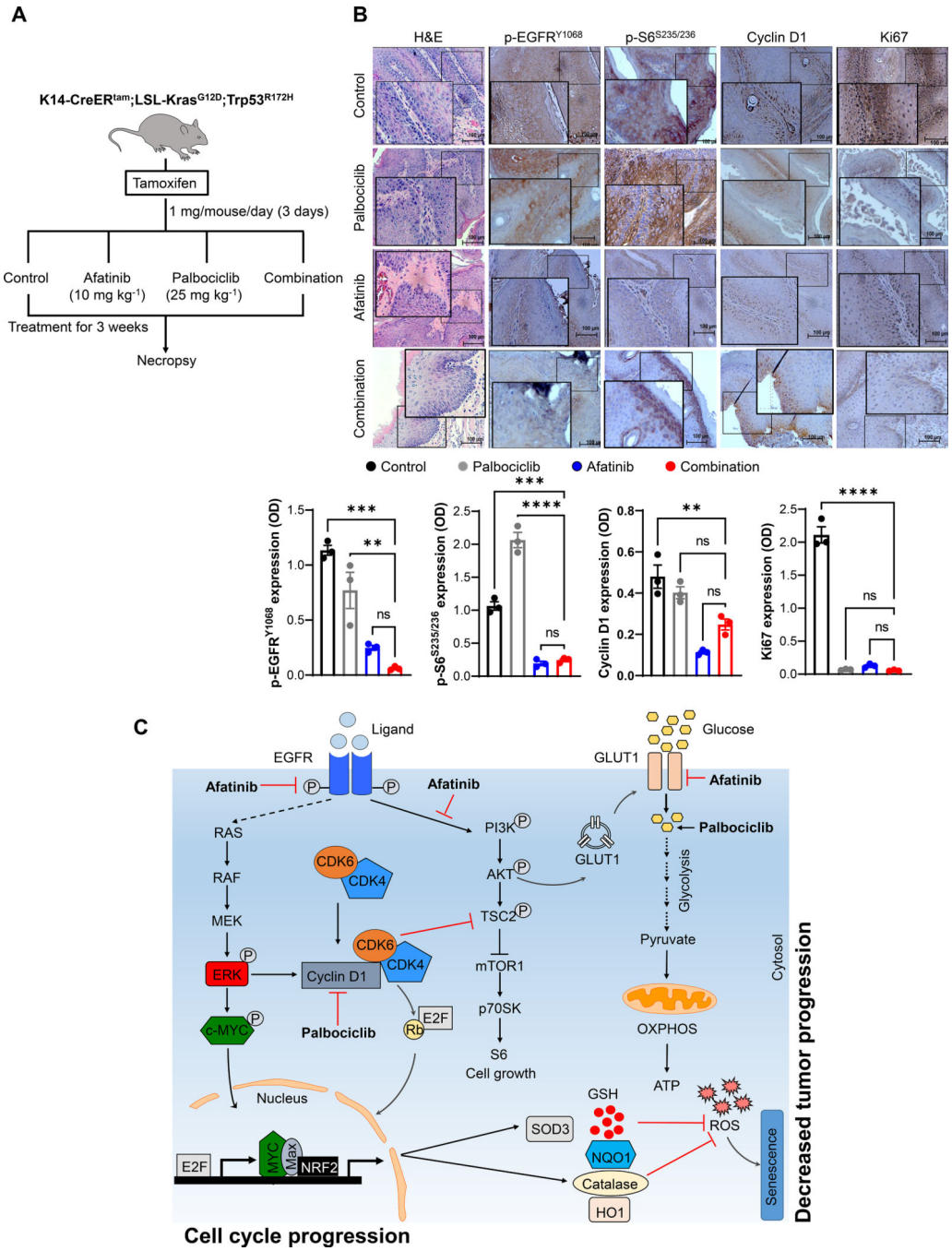

Fig. 6. Combination treatment delays HNSCC progression in a GEM model.

a. Schema of drug treatment strategy in GEM model (left panel). Ten days after Cre activation, KKP mice (K14-CreER^{tam};LSL-Kras^{G12D};Trp53^{R172H}) treated with palbociclib (25 mg/kg/day), afatinib (10 mg/kg/day), combination or vehicle control for 21 days. Mice sacrificed and oral tissues analyzed by H&E. **b.** Immunohistochemistry of p-EGFR (Tyr-1068), p-S6 (Ser-235/236), cyclin D1, and Ki67 in KKP tumors after treatments (n=3). Image scale = 100 μm. The positive staining (OD) of the respective proteins is provided (bottom panel). c. Current proposed model of how combination therapy block tumor

progression. Targeting CDK4/6 with palbociclib activates Rb to induce cell cycle arrest. However, palbociclib also activates EGFR to increases cyclin D1 and E1 levels. And afatinib inhibits EGFR signaling and decreases cyclin D1, cyclin E1, and p-S6 (Ser-235/236) expression. In contrast, combination treatment reduces the glucose uptake and inhibits both glycolysis and TCA cycle with no change in OXPHOS. Furthermore, decreased SOD3, NQO1, NRF2, and catalase levels by combination lead to increased ROS levels, mitochondrial dysfunction and metabolic alteration, resulting in cellular senescence with an overall decrease in tumor growth and development. Data represent mean ± SEM. ANOVA followed by Tukey's multiple comparisons test was used between groups (**b**). **P < 0.01, ***P < 0.001, ****P < 0.0001, and ns=non-significant. OD=optical density.

Key Resource Table

REAGENT	SOURCE	IDENTIFIER
Antibodies		
p-Rb (Ser-807/811), WB: 1:1000	Cell Signaling Technology	Cat#9308
p-EGFR (Tyr-1068), WB-1:1000, IHC- 1:300	Cell Signaling Technology	Cat#2234
EGFR, WB-1:1000	Cell Signaling Technology	Cat#2232
p-S6 (Ser-235/236), WB-1:1000, IHC-:200	Cell Signaling Technology	Cat#4858
p-p70SK (Thr-371), WB-1:1000	Cell Signaling Technology	Cat#9208
p-p70SK (Thr-389), WB-1:1000	Cell Signaling Technology	Cat#9205
ERK1/2, WB-1:1000	Cell Signaling Technology	Cat#9102
mTOR1, WB-1:1000	Cell Signaling Technology	Cat#2983
p-mTOR1 (Ser-2448), WB-1:1000	Cell Signaling Technology	Cat#2971
p-Akt (Ser-473), WB:1:1000	Cell Signaling Technology	Cat#4060
Akt, WB:1:1000	Cell Signaling Technology	Cat#2920
p-ERK (Thr-202/Tyr-204), WB:1:1000	Cell Signaling Technology	Cat#4370
Cyclin D1, WB-1:300, IHC:1:100	Santa Cruz	Cat#sc-8396
Cyclin E1, WB-1:300	Santa Cruz	Cat#sc-377100
CDK4, WB-1:300	Santa Cruz	Cat#sc-23896
CDK6, WB-1:300	Santa Cruz	Cat#sc-7961
Rb, WB-1:300	Santa Cruz	Cat#sc-102
p-Rb (Ser-780), WB-1:300, IHC-1:100	Santa Cruz	Cat#sc-12901
SOD1, WB-1:300	Santa Cruz	Cat#sc-101523
SOD2, WB-1:300	Santa Cruz	Cat#sc-137254
SOD3, WB-1:300	Santa Cruz	Cat#sc-271170
NQO1, WB-1:300	Santa Cruz	Cat#sc-32793
Tom20, IF-1:250	Santa Cruz	Cat#sc-17764
β-actin, WB-1:500	Santa Cruz	Cat#sc-517582
OXPHOS, WB-1:250	Abcam	Cat#ab110413
NRF2, WB-1:1000	Abcam	Cat#ab137550
Keap 1, WB-1:1000	Abcam	Cat#ab119403
Catalase, WB-1:1000	Abcam	Cat#ab16731
Ki67, IHC-1:200	Abcam	Cat#ab15580
OXPHOS, WB-1:1000	Abcam	Cat#ab110411
cMyc, WB-1:1000	Abcam	Cat#ab152146
p-cMyc (Ser-62), WB-1:1000	Abcam	Cat#ab185656
p-cMyc (Thr-58), WB-1:1000	Abcam	Cat#ab185655
FOXM1, WB-1:1000	Abcam	Cat#ab180710
GLUT1, wb-1:1000	Novas Biologicals	Cat# NB110-39113
Kits and Chemicals		
Glucose Uptake Cell-Based Assay	Cayman Chemicals	Cat#600470

REAGENT	SOURCE	IDENTIFIER
ATP Detection Assay Kit-Luminescence	Cayman Chemicals	Cat#700410
MitoProbe JC-1 Assay Kit	Thermo Scientific	Cat#M34152
MitoSOX™ Red Mitochondrial Superoxide Indicator, for live-cell imaging	Thermo Scientific	Cat# M36008
Fluorometric Intracellular Ros Kit	Sigma-Aldrich	Cat#MAK145
DAB Peroxidase (HRP) Substrate Kit (with Nickel), 3,3'-diaminobenzidine	Vector Laboratories	Cat#SK-4100
Palbociclib (PD-0332991) HCl	Selleckchem	Cat#S1116
Afatinib (BIBW2992)	Selleckchem	Cat#S1011
N-Acetyl-L-cysteine	Sigma-Aldrich	Cat#A9165
Glutaraldehyde solution	Millipore Sigma	Cat#G7776
X-Gal	ThermoFisher Scientific	Cat#B1690
Potassium ferrocyanide trihydrate	Acros Organics	424130050
Potassium ferricyanide	Acros Organics	223111000
Thiazolyl blue tetrazolium bromide	Acros Organics	158990050